IEEE Access
Multidisciplinary ⋮ Rapid Review ⋮ Open Access Journal

Received July 19, 2021, accepted August 13, 2021, date of publication August 20, 2021, date of current version August 27, 2021.

Digital Object Identifier 10.1109/ACCESS.2021.3106319

A Low-Profile Vacuum Actuator (LPVAc) With Integrated Inductive Displacement Sensing for a Novel Sit-to-Stand Assist Exosuit

ASITHA L. KULASEKERA[1], (Member, IEEE), RANCIMAL B. ARUMATHANTHRI[1], DAMITH S. CHATHURANGA[1], (Member, IEEE), R. A. R. C. GOPURA[2], (Senior Member, IEEE), AND THILINA D. LALITHARATNE[3], (Member, IEEE)

[1]Computational Sensing and Smart Machines (CSSM) Laboratory, Department of Mechanical Engineering, University of Moratuwa, Moratuwa 10400, Sri Lanka
[2]Bionics Laboratory, Department of Mechanical Engineering, University of Moratuwa, Moratuwa 10400, Sri Lanka
[3]Dyson School of Design Engineering, Imperial College London, London SW7 9EG, U.K.

Corresponding author: Asitha L. Kulasekera (asitha@uom.lk)

This work was supported in part by the National Research Council of Sri Lanka under Grant 17-018, and in part by the University of Moratuwa, Senate Research Committee under Grant SRC/TP/2017/10.

This work involved human subjects or animals in its research. The authors confirm that all human/animal subject research procedures and protocols are exempt from review board approval.

ABSTRACT Muscle weakness owing to stroke, spinal cord injuries, or aging can make a person's life sedentary, temporarily as well as permanently. Such persons need to be motivated to break their sedentary postures and attempt independent motion. A key motivator in this aspect is the ability to easily transition from seated to standing posture. If this sit-to-stand transition (STSt) is easy, it will encourage further mobility. A soft wearable device that can assist the STSt, would fill this need perfectly. Such a device should be able to seamlessly assist during STSt and be unobtrusive during sitting. A major limitation that is currently holding back the development of soft exosuits in STSt-assist is the lack of low-profile soft actuators with high strain rate and force-to-weight ratio. Hence, we propose a novel low-profile vacuum actuator (LPVAc) with an integrated inductive displacement sensor that, can be rapidly fabricated, is lightweight (14 g), and can provide high strain (65%) and a high force-to-weight ratio (285 times self-weight). The proposed actuator comprises a low-profile spring encased within a low-density polyethylene film with rapid vacuum actuation and passive quick return. The proposed inductive sensor has a sensitivity of 0.0022 $\mu H/mm$ and the hysteresis is below 1.5% with an overall absolute average error percentage of 5.24%. The performance of the proposed integrated sensor in displacement control of the LPVAc is experimentally evaluated. The proposed actuator is integrated into a novel mono-articular STSt-assist exosuit for preliminary testing. Surface electromyography measurements of the gluteus maximus muscles during STSt indicate a mean muscle activity reduction of 45%. This supports the potential use of the proposed actuator in STSt-assist.

INDEX TERMS Actuators, exoskeletons, exosuits, inductance measurement, orthotics, sensors, soft sensors, soft robotics, vacuum systems.

I. INTRODUCTION

The quality of life (QoL) of an individual depends on that person's ability to independently carry out activities of daily living (ADL), such as dressing/bathing, eating, walking and toileting without difficulty [1]. Functional mobility, or walking, is a key ADL, that greatly influences a person's functional independence and health-related quality of life. Hence, lower limb muscle weakness, can drastically affect the health and livelihood of a person, cause subsequent medical disorders, and lead to physical and psychological dependency [2].

Diseases such as stroke, accidental trauma such as spinal cord injuries, can temporarily or permanently reduce and/or limit a person's mobility. Age and obesity can also have a detrimental effect on functional mobility. In both the above situations, promoting the patient to attempt independent motion is advantageous in recovery [3]. Hence, they must be encouraged to break their sedentary posture and attempt

The associate editor coordinating the review of this manuscript and approving it for publication was Yingxiang Liu.

independent motion. In achieving this independent motion, the major obstacle is the initial transition from seated posture to standing posture. This sit-to-stand transition(STSt) relies heavily on the muscle strength of the lower limb. Hence, lower limb muscle weakness can significantly demotivate repeated STSt, thus leading to secondary health complications. One way to break this vicious cycle is to provide the person with assistance during the STSt, which would encourage the person to repeatedly attempt independent STSt. This would lead to frequent attempts at independent walking, which in turn would reduce secondary complications associated with a sedentary lifestyle and have improved QoL [3].

Rigid exoskeleton systems have been the preferred robotic assistance solution in the recent past. Though significant research has been done on rigid robotic exoskeleton systems [4]–[6], several inherent drawbacks limit their use as truly wearable systems. Rigid exoskeletons tend to be bulky and have limited application in distal positions due to the addition of extra inertial loads. This can lead to deviation from natural motion and create subsequent pain due to axial misalignments [7]. The added inertial load can lead to increased metabolic cost [8] and could potentially result in cartilage damage [9]. These limitations ultimately lead to increased wearer discomfort and will in turn limit the wearer from donning the device for a longer duration [5]. Hence, there is a clear requirement for a better wearable assist solution that can address these limitations posed by rigid systems.

The exosuit concept has been presented in the literature recently, as an effective alternative to rigid exoskeletons. An "exosuit" is a soft wearable device, that can even be easily worn under normal clothing, that can provide assistive or augmentative forces to the wearer's limbs. In contrast to rigid exoskeletons, which provide torque across limb joints, the exosuit attempts mimic the muscular actuation by delivering forces parallel to the muscles. Recent exosuit research has focused on integrating novel functional textiles, soft actuators, soft sensors, flexible power systems, and control strategies to provide seamless human-machine interaction [10]–[12]. Most of the exosuits found in the literature have concentrated on general gait assistance such as plantar/dorsiflexion
assist [12], [13] and hip flexion assist [14]–[16] in post-stroke patients. Only a few have attempted assisting anti-gravity muscles during activities such as sit-to-stand, stair climbing and descending [3], [17].

In this paper, we propose a novel low-profile vacuum actuator (LPVAc) with an integrated inductive displacement sensor (see Fig. 1). Part of this work has been previously presented in our recent conference publications [18], [19]. This work extends to further in-depth characterization and performance analysis of the proposed actuator and the integrated sensor. The proposed actuator, can be rapidly fabricated, is lightweight, can provide high strain and high force-to-weight ratio, and has an integrated displacement sensor. It comprises a low-profile spring encased within a low-density polyethylene (LDPE) film. The design provides

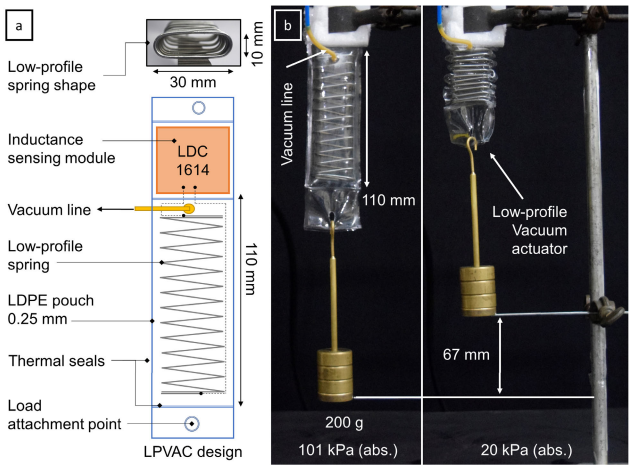

FIGURE 1. The composition and operation of the LPVAc. a) The LPVAc comprises an LDPE pouch of 0.25 mm thickness, encasing a 110 mm long obround-shaped low-profile (30 mm × 10 mm) spring. An LDC1614 module is integrated to provide inductive displacement sensing. The spring is electrically connected to the inductance measurement module. b) The LPVAc lifting a 200 g load 67 mm at 20 kPa (abs.) vacuum pressure.

rapid vacuum actuation and passive quick return. Furthermore, an inductive sensing method is integrated into the proposed actuator and its performance and characteristics are experimentally evaluated. The performance of the proposed integrated sensor in displacement control of the LPVAc was experimentally evaluated as well. Finally, a preliminary prototype of a novel STSt-assist mono-articular exosuit driven by the proposed actuator is experimentally tested to evaluate the assist capability of the actuator for STSt. The rest of the paper is comprised as follows; Section II describes the recent related work in the development of low-profile soft actuators, integrated soft sensing, and exosuits; The design and fabrication of the proposed actuator and the sensor integration is presented in Section III. The experimental evaluations and their results are described in section IV. The preliminary testing of a STSt-assist exosuit driven by the proposed actuator is shown in Section V. Section VI presents the conclusions.

II. RELATED WORK

The following sections present contemporary research on the areas related to soft actuators, their integrated sensing development, and exosuits for sit-to-stand assistance.

Soft robotics has become a disruptive technology that has been recently proposed to overcome the limitations of contemporary rigid robotic systems. Soft robotics aims to replace the rigid and hard components of conventional robotic systems with soft and flexible components. In contrast to metallic structures of traditional robots, a soft robot would incorporate soft and easily deformable materials (i.e., polymers, latex rubber, silicone rubber, etc.) [20]. Though conventional rigid robots excel in industrial applications due to their power and precision, they are at a disadvantage when it comes to delivering safe human-robot interactions [20], [21]. With the growing interest in recent years towards the development

of robotic solutions for human assistance, healthcare and wearable devices, safety has become critical over, power and precision. While conventional rigid robotic systems would have to rely on complex control protocols and algorithms to work with humans in the same environment, soft robots are able to offer intrinsically safer human interactions due to their inherent compliance [22], [23].

Actuators, sensors, structures, and control systems can be considered to be the main components in any robotic system. A soft robotic solution would attempt to provide all or some of these components, through soft, flexible components. Pneumatic artificial muscles (PAMs) are a commonly used type of actuator in soft robotics. A PAM would utilize pneumatic input to deliver contractile, tensile, bending, or rotary motion/force. The McKibben muscle is a renowned example for a PAM, with a history dating back to the 1950's [24]. Modern McKibben type PAMs have been developed for industrial applications, with the ability to deliver forces up to 3.5 kN from an actuator of 20 cm length [25]. Several other PAM designs can be found in the recent literature, such as fiber-reinforced PAMs [26], [27], bellows-type PAMs [28], flat PAMs with zero-volume cavities [29], and thin McKibben type PAMs [30].

Advantages such as inherent safety, being lightweight, having lower mechanical constraints, compactness, having a higher power-to-weight ratio in comparison to rigid counterparts, the ability to rapidly delivering required motion/force have made PAMs a strong candidate for use in wearable robotic systems [24], [29], [31], [32]. Recent literature presents wearable devices that utilize PAMs for finger movements [33], [34] and knee, ankle movements [35], lower-limb exoskeletons [10], [36]. However, most contemporary PAMs capable of powering wearable devices have a large cross-sectional area due to their cylindrical shape. This limits the ability to integrate the PAM into wearable devices without being obvious and obstructing. Hence, there exists a need to develop low-profile PAMs suited for easy integration to wearable systems such as exosuits [10].

A. CONTRACTILE VACUUM ACTUATORS

PAMs offer an attractive solution for wearable assistive device development due to their high force-to-weight ratio, hygienic operation close to humans and good human safety due to similar contraction properties and compliance characteristics to biological muscles [37], [38]. Research on PAM development has been more focused on using positive pressure for actuation, with growing recent interest in utilizing negative pressure (vacuum, below external) [39]–[42]. Vacuum-driven actuators possess several distinctive, inherent advantages, over positive pressure actuators. They pose no risk of explosion or bursting, they reduce in volume while in operation allowing them to be effectively used in confined spaces, have large contraction ratios, can be rapidly actuated, and are highly robust towards leakages and seal ruptures [39], [40]. One of the few main limitations is that the maximum applicable forces and displacements are limited by the maximum vacuum pressure (of 0 Pa (abs.)) unless hyperbaric conditions are used.

Vacuum PAMs (VPAMs) undergo volume reduction during actuation, unlike conventional PAMs, leading them to be called inverse PAMs. VPAMs typically are actuated by evacuating a fluid within a cavity of a deformable structure using a negative pressure source. During this evacuation, the structure will collapse, producing a contraction and hence, a tensile force. Maximum force generation in this scenario depends on limiting the structural collapse to the longitudinal direction. Recent literature presents few methods/designs that allow for this. One such method is the controlled collapse of elastomeric cellular cavity structures using the theory of buckling of columns [39]. This concept utilizes thick cross-beams made of silicone rubber material that allows controlled collapse along the direction of the columns. The use of the elastomer also allows for shock absorbance and elastic energy storage during actuation and return. The need for thick beams and large cavity volumes are two main limitations of this method. Secondly, an elastomer-covered foam core has been utilized as the collapsible volume [43]. The elastomer creates a closed volume for vacuum actuation. Upon connection to vacuum pressure, the air inside the foam core is removed, collapsing the structure. The foam structure also acts as elastic energy storage that assists the return of the actuator to the neutral state. Thirdly, the method of most interest recently is the collapse of an inextensible film pouch where a rigid/semi-rigid skeletal structure guides the collapse [40]–[42], [44]. In this method, a collapsible skeletal structure controls the collapse of an inextensible fluid-tight thin-walled pouch. Several skeletal structures has been proposed, such as 3D-printed zigzag structures [40], rings/cross-section supports [41], [44] and spine/vertebrae like structures [42].

B. INTEGRATED SENSING

Though PAMs show incredible promise in the development of soft robotic applications, the absence of integrated force and displacement feedback solutions, is currently holding them back. The presence of such integrated force and displacement feedback solutions would allow PAMs to achieve effective closed-loop control. Some PAMs have tried integrating encoders [24], potentiometers [45], flexible force-sensing resistors [46] and hall effect sensors [47] for displacement feedback. Strain [48] and gauge pressure [49] sensing, has been used for obtaining force feedback. Yet, as these methods include rigid and semi-rigid mechanisms, they add extra weight, affect the required motion of the actuator and negatively affect the advantages of the actuator being soft. The use of conductive liquid metal sensors has also been proposed as a much softer feedback sensing solution. Channels filled with Ga-In alloys have been used to provide feedback on the actuator deformation [50], [51]. These channels can alter the desired deformation of the actuator. Further, any damage to the channel will lead to the leakage of the liquid metal compromising the performance of the sensor.

C. EXOSUITS FOR SIT-TO-STAND ASSISTANCE

Sit-to-stand transition (STSt) assist exosuits [3], [17] have become of interest in the recent literature with the growing aging populations worldwide. STSt is an anti-gravity muscle activity, that starts from a seated posture and ends with the person standing straight. Hence, during the initial part of STSt, the wearable assist system needs to allow for comfortable seating. Therefore, the actuators in the STSt assist exosuit, as well as the exosuit itself, is best to be soft and flexible. Actuators with large cross-sections will limit the comfortability during the seated phase, hence, they should be low-profile to improve wearer comfort. The use of heavy actuators that can deliver large forces will put an unnecessary inertial penalty on the wearer, therefore, an efficient strategy is to use soft, low-profile actuators with a high force-to-weight ratio.

Contemporary STSt assist exosuits in the literature have relied on the use of motor-driven cables as the actuating mechanism. The common design strategy for the exosuit has been to use inextensible webbing straps to acts as fixturing, anchoring, and force directing pathways. The use of webbing straps in this manner is a common exosuit design strategy, which utilizes the lines of non-extension described in [10]. The Bartenbach exosuit uses a hip-mounted motor system to provide assistive forces using a Bowden cable [3]. Here, the webbing straps are anchored to the pelvis and the ankle. As a passive exosuit prototype, the Bartenbach design describes the conceptual use of an exosuit in anti-gravity STSt assist. Schmidt exosuit presented in [17], extends the above design to an experimental prototype that reports reduction in knee and hip extensor muscle activity during STSt for the first time. In the Schmidt design, they use a Dyneema cable driven by a shank-mounted DC motor assembly. Their proposed suit weighs 4.56 kg with batteries, with the shank-mounted subsystem weighing 1.07 kg per leg. This work shows that it is possible to deliver STSt assistance using a soft exosuit reducing the required muscle activity.

III. DESIGN AND FABRICATION OF THE LPVAc

We propose a novel low-profile actuator design, that combines an obround-shaped spring, enclosed within a flexible, thin-walled minimally extensible film pouch, integrated with a displacement sensor. The contraction is created by the evacuation of the air inside the actuator, by connecting it to a negative pressure source. If this evacuation is done simply on a pouch, the film layers on opposite sides of the pouch will collapse on top of each other. This uncontrolled collapse would limit the effectiveness of the contraction and limit the return to the initial state unless inflated with a positive pressure airflow. Therefore, a spring is used to act as an integrated skeletal structure, similar to those of the origami-inspired VPAMs, that would both direct the film pouch collapse longitudinally, and assist in a quick return to an un-actuated state once the vacuum source is disconnected. Here, we propose the use of an obround-shaped helical spring, as opposed to the typical circular cross-sectioned springs, to reduce the cross-sectional diameter to obtain a low-profile actuator. This would allow the proposed actuator for improved integration with wearable exosuit designs that would have minimal obstruction/pose minimal discomfort to the wearer. In order to obtain position feedback from the actuator, we propose the use of inductive sensing of the contraction of the spring. Hence, a commercially available inductance sensing module is integrated into the actuator, within the LDPE pouch, to measure the change of the spring inductance during actuation.

A. LPVAc FABRICATION

The fabrication process of the proposed LPVAc is described in this section. The low-profile spring that acts as the skeletal structure and the thin film pouch are the two main components. The design of the proposed low-profile spring is of an obround shape, see Fig. 1, with a width three times that of the height. This spring design is based on the typical loading spring found on a gun magazine. This low-profile spring can be manufactured using traditional fabrication methods, by winding over a rectangular block and heat treating to program in the required shape. Galvanized iron (GI) and mild steel (MS) were selected for the prototype spring fabrication due to the ease of fabrication offered by those materials. The performance of these springs was experimentally evaluated to understand their spring characteristics. The helical design consists of 11 effective turns over a 100 mm length, and uses a 1.2 mm wire. The dimensions of the fabricated low-profile spring are shown in Fig. 1. The low-profileness of the actuator can be defined as,

$$Low\ Profileness = Width/Height \tag{1}$$

The shown low-profile spring in Fig. 1 has cross-section dimensions of 30 mm $\times$ 10 mm. Hence, this spring has a $Low-profileness$ or $width/height$ ratio of three. Another two low-profile actuators of differing $width/height$ ratios were fabricated to see the effect of the low-profileness on the deliverable force.

Low-density polyethylene (LDPE) film was selected to create the inextensible, thin-walled pouch, due to its previous success [40], [42] as well as the common-place availability, and ease of fabrication. To fabricate the pouch, rectangular film strips were cut. The strip length was calculated to include the spring length of 100 mm, allowances for the actuator height of 10 mm and warping when creating the thermal seals and additional customizable length for attachment purposes (minimum total length: 110 mm). The fabrication steps for the actuator are as follows:

1) Place two rectangular LDPE layers on top of one another.
2) Create a longitudinal seal using the thermal sealer.
3) Place the low-profile spring within the created fold.
4) Mark the placements for the vacuum line and the top and bottom seals. (Vacuum line inlet is placed near the top of the spring, intentionally between spring turns to

prevent closing up of the line by the spring or collapsing film during actuation.)

5) Punch in a tiny hole using a needle for the vacuum line inlet.
6) Insert a latex tube through the punched hole and seal using a cyanoacrylate adhesive.
7) Create the second longitudinal seal.
8) Create the top and bottom seals creating the pouch with enclosed air volume.
9) Additional thermal seals can be made at the ends of the film layer sections to provide allowances for attachments.
10) Add grommets to the actuator for easy attachment/fixing.

The inductance sensing module is integrated within a separate pouch on the top of the LPVAc (see Fig. 1). The top and bottom ends of the metal spring was connected to the evaluation module using thin insulated wire to ensure minimum disturbance to the actuator. The fully fabricated actuator weighs only 14 g without the sensing module.

B. SENSOR WORKING PRINCIPLE

A metal spring can be used as a sensor since the spring's inductance varies directly with its length [52]. Therefore this property can be used to measure the displacement of a spring. Here an inductance to digital converter (LDC 1614, Texas Instruments) was used to get the inductance value of the low profile spring of the actuator. The spring (inductor) and a capacitor (1nF) is connected in parallel so that LC tank circuit can be achieved and the oscillating frequency is measured by the evaluation module. The inductance measurement module gives an inductance (*DATA*) value as a ratio of the sensor frequency f_{sensor} with respect to a reference frequency f_{ref}. The sensor frequency is the frequency at which the LC tank oscillates. f_{ref} was set to 43 Mhz. The LDC1614 module datasheet [53] gives this relationship as shown in (2).

$$\frac{DATA}{2^{28}} = \frac{f_{sensor}}{f_{ref}} \tag{2}$$

Also,

$$f_{sensor} = \frac{1}{2\pi\sqrt{LC}} \tag{3}$$

where L is the inductance value and C is the capacitor value. By adding the values for equations (1) and (2) it can be simplified to

$$L = \frac{9.69}{DATA^2} * 10^6[\mu H] \tag{4}$$

Using (4), the inductance of the spring was obtained, and by plotting the inductance vs displacement curve, then sensor calibration was done. The LDC1614 module has a 28-bit resolution, hence for the given configuration, it is able to provide a step size close to 10 nH [53].

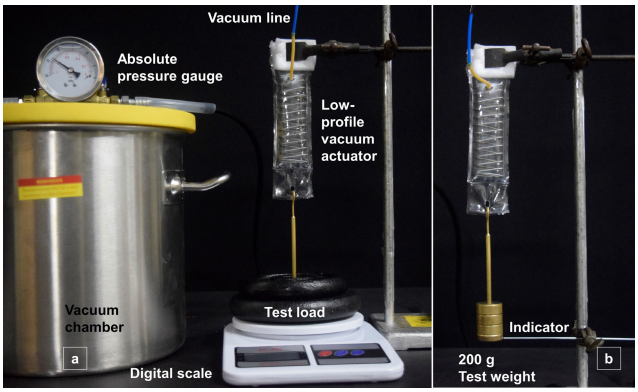

FIGURE 2. The experimental test setups used for actuator characterization. (a) maximum force evaluation, (b) displacement evaluation.

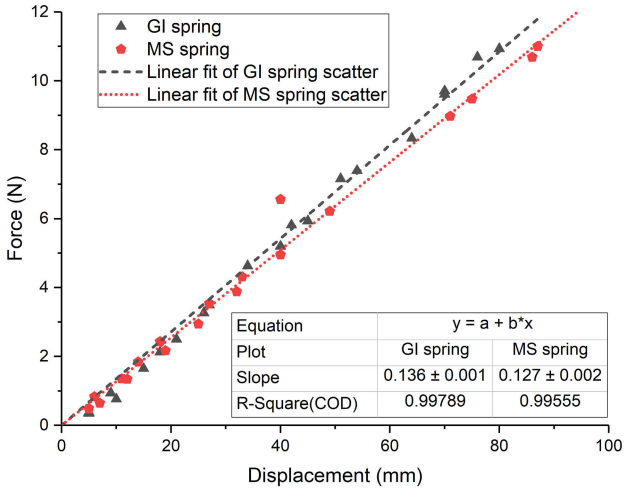

FIGURE 3. The experimental force-displacement characteristics of galvanized iron (GI) and mild steel (MS) obround-shaped low-profile springs. The results show that it is valid to assume a conventional helical spring model to describe the behavior of the obround-shaped helical spring.

IV. EXPERIMENTAL EVALUATION OF THE LPVAc AND INTEGRATED SENSOR

The experimental test setup is shown in Fig. 2 was used to obtain the isometric and isotonic characteristics of the proposed LPVAc as described in the following subsections.

A. SPRING COEFFICIENT OF THE LOW-PROFILE SPRING

The behavior of the low-profile spring was initially considered to be different from that of a common circular helical spring. The deflection of the spring under axial load and developed stresses may be affected by the obround (stadium) shaped cross-section in the selected low-profile spring [54]. Therefore, preliminary experiments were carried out to evaluate the force-displacement characteristics of the low-profile spring. The experimental results (Fig. 3) show that it is acceptable to assume standard Hooke's law, $F_{spring} = -kx$, for the obround shaped low-profile spring as well. The spring coefficients for the tested springs were calculated as follows: MS: 127 N/m and GI: 136 N/m.

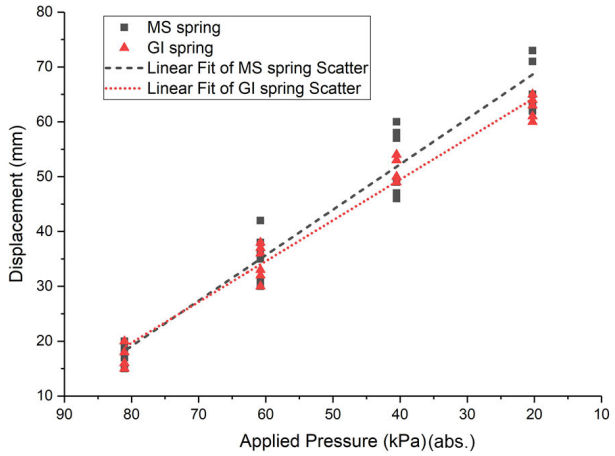

FIGURE 4. The observed displacement observed with varying vacuum pressure for a test load of 200 g. Values are shown for galvanized iron (GI) and mild steel (MS) spring-based actuators.

B. LPVAc CONTRACTION WITH VACUUM PRESSURE

The load-displacement characteristics of the proposed LPVAcs were evaluated using the experimental setup shown in Fig. 2(B). The isotonic characterization was carried out with a fixed attached load with varied applied vacuum pressure. Fig. 4, presents the load-displacement characteristics for an attached load of 200 g. The experimental results show a linear correlation between the displacement with increasing applied vacuum pressure. The MS spring-based actuators showed slightly higher displacement performance at higher vacuum pressures compared to the GI spring-based LPVAc. A maximum strain of 65 % (contraction ratio: 182 %) was observed at no-load condition at a vacuum pressure of 20 kPa (abs.) (see Fig. 5).

C. LPVAc FORCE-DISPLACEMENT CHARACTERISTICS

The force-displacement characteristics of the proposed LPVAcs were evaluated using the experimental setup shown in Fig. 2(B). MS spring-based LPVAc were evaluated due to their better displacement performance shown in Fig. 4. The attached load was varied up to 20 N, with varied vacuum pressure from 60 kPa (abs.) to 10 kPa (abs.). The results obtained (see Fig. 6) show that the force-displacement characteristics are scalable with increasing vacuum pressure.

D. MAXIMUM BLOCKED FORCE VARIATION

The maximum blocked force performance of the proposed LPVAc was evaluated using the experimental setup shown in Fig. 2(A). LPVAcs were fixed to the test frame and was attached to a test load put on a digital scale. This test load acts as a blocking force when the LPVAc is actuated. The digital scale reading was set to zero after the test loads were placed. Once the LPVAc was actuated, the scale records applied blocked force as a negative reading. This reading was recorded as the maximum blocked force of the actuator. The experimental blocked force readings (Fig. 7), show a linear correlation with blocked force with varied applied vacuum pressure.

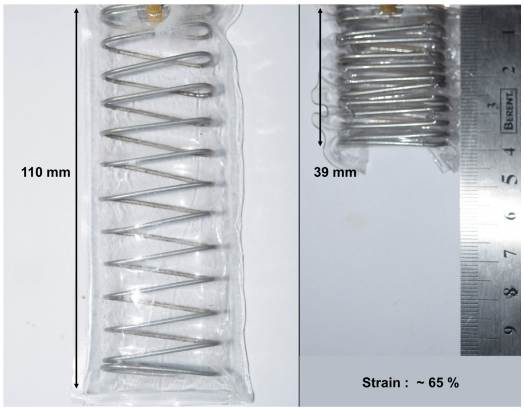

FIGURE 5. The LPVAc produces a maximum strain of 65% at 20 kPa (abs.)

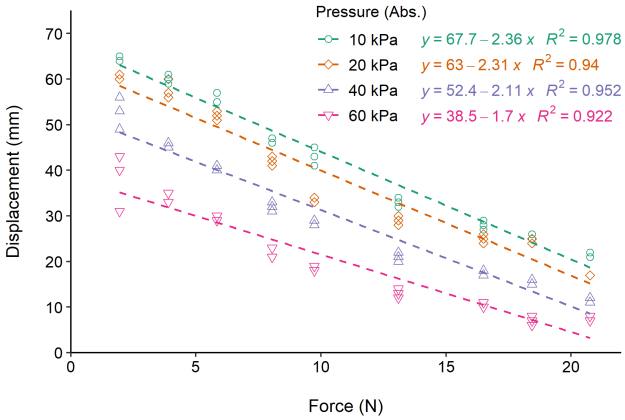

FIGURE 6. The change in displacement with varying attached load for multiple pressure (absolute) levels. The dashed lines indicate the linear regression fits obtained using the least squares method for the experimental values given by the markers.

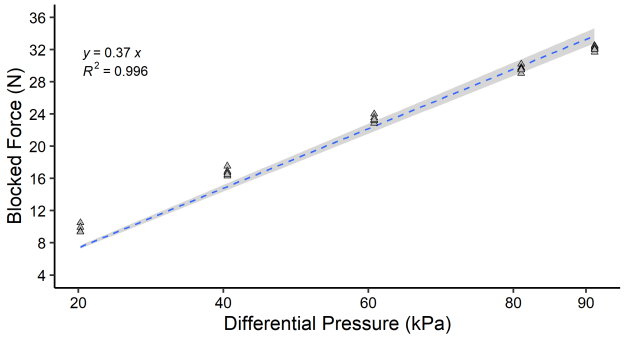

FIGURE 7. The blocked force performance of the LPVAc (using spring #1) with varying applied differential pressure. The shaded area show the 95% confidence interval for the least squares fit.

E. EFFECT OF WIDTH-TO-HEIGHT RATIO ON BLOCKED FORCE PERFORMANCE

To study the effect of low-profileness on the blocked force performance of the LPVAc, two more low-profile springs were produced with different width and height combinations (see Fig. 8). New LPVAcs using these new springs were manufactured following the same method described earlier.

	Spring #2	Spring #1	Spring #3
W x H (mm)	30 x 15	30 x 10	40 x 10
W/H	2	3	4
Cross-section area (mm²)	402	279	379

FIGURE 8. The dimensions and the characteristics of the low-profile obround springs made with differing width/height ratios.

TABLE 1. LPVAc performance with varying W/H ratio.

Spring #	W/H	Maximum Output Force (N)	Maximum Output Stress (kPa)	Force-to-weight ratio
1	3	32.5	79	237
2	2	29	80.7	212
3	4	39.05	103.2	285

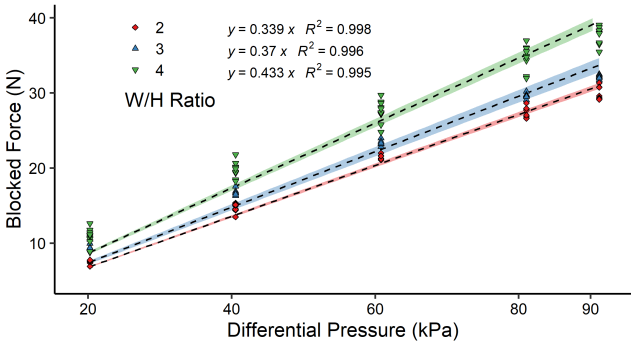

FIGURE 9. The blocked force performance of the LPVAc with varying W/H ratio. The shaded area shows the 95% confidence interval for the least squares fit.

As the W/H ratio increases, the curved surface area of the LPVAc reduces and increases the flat rectangular area. The blocked force performance of these spring combinations was tested as earlier. The performance of each LPVAc with a different W/H ratio is shown in Table 1.

It is observed that (Fig. 9), there is an increase in the blocked force with increasing differential pressure as the W/H ratio is increased. The increased rectangular area of the LPVAc with the increasing W/H ratio may be the cause for the increasing blocked force performance.

F. SENSOR CALIBRATION

The experimental evaluation carried out to calculate the sensor equation is described in this section. The spring inductance was measured via the LDC1614 module as the LPVAc was actuated. The collected results are shown in Fig. 10. The least-squares method was used to derive a relationship between the measured spring inductance (L) vs the actuator displacement (D). Fig. 10 shows this relationship to be highly linear, with R^2 of 0.97. The calculated sensor equation is shown in the equation (5), where D is in mm and L is in μH.

$$L = 0.0022\,D + 0.75 \tag{5}$$

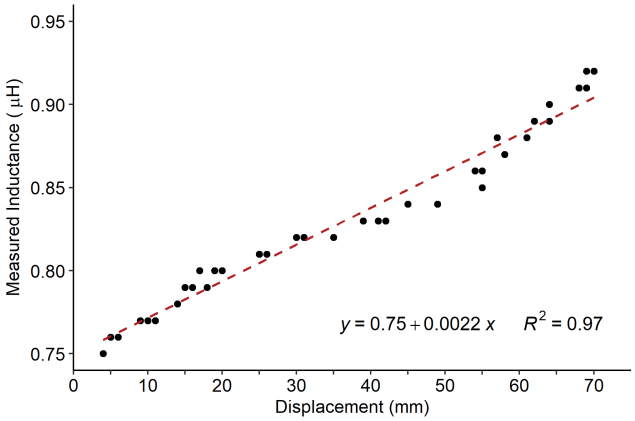

FIGURE 10. The least-squares fit obtained for the measured inductance vs. the actuator displacement.

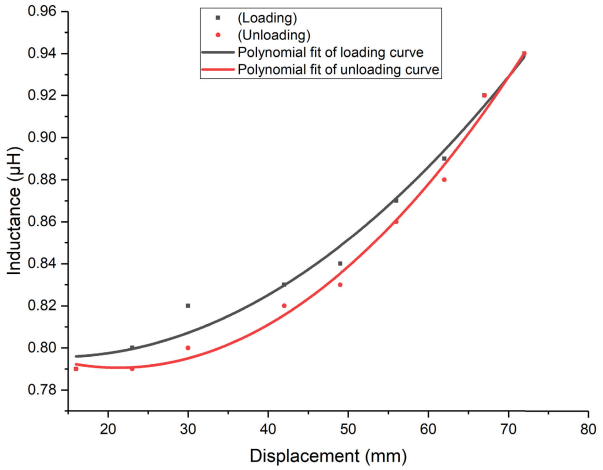

FIGURE 11. The sensor performance during loading and unloading.

G. HYSTERESIS AND REPEATABILITY

The LPVAc was actuated and released by increasing and decreasing the vacuum pressure to evaluate the hysteresis performance. The hysteresis performance of the sensor is shown in Fig. 11. The observed hysteresis is calculated as 1.49%. Repeated measurements at preset positions were made to assess the repeatability of the sensor. The LPVAc was contracted to three preset positions [48 mm, 60 mm, and 72 mm] and repeated readings were taken for 20 iterations at each position. The variation of the sensor output with the measurement number is shown in Fig. 12. A statistical analysis of these measurements is given in Table 2. The sensor shows good repeatability with standard deviations of 2.35 mm, 2.3 mm, and 1.65 mm for each of the preset positions, respectively.

H. SENSITIVITY AND MEASUREMENT ERROR

The sensitivity of a sensor can be obtained using its transfer function. Hence, from the slope of the transfer function, the sensor sensitivity was found to be 0.0022 $\mu H/mm$

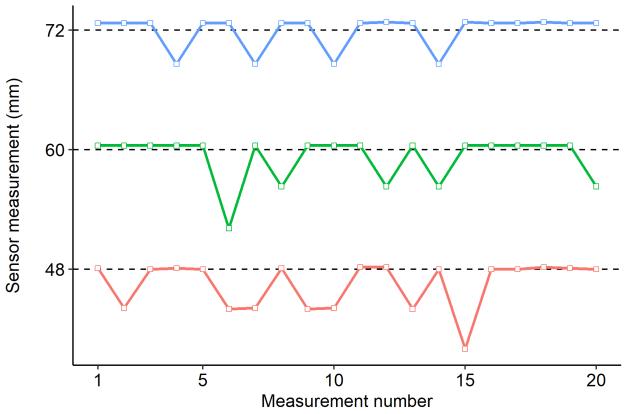

FIGURE 12. The repeatability performance of the inductive displacement sensor for three [48, 60, and 72 mm] preset displacement positions (n = 20).

TABLE 2. Performance measures for repeatability of the sensor.

No. of Iterations	Test 1	Test 2	Test 3
	20 *iterations*		
Preset contraction [mm]	72	60	48
Mean sensor reading [mm]	71.9	59.17	46.47
Std. deviation [mm]	1.65	2.3	2.35
Mean error [mm]	1.9	-0.84	-1.54
Measurements $\leq$ 5 % error [%]	80	75	65
Measurements $\leq$ 10 % error [%]	100	95	95

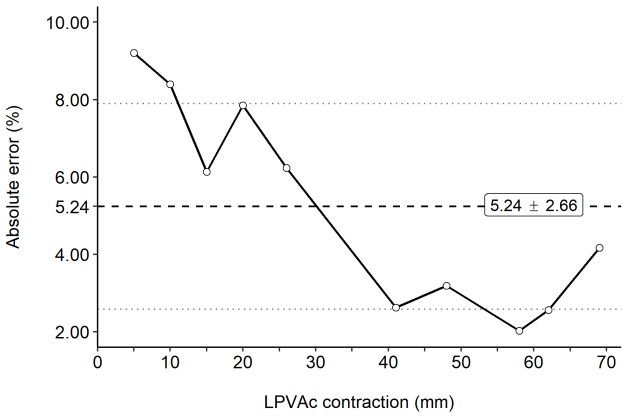

FIGURE 13. The observed sensor error over the LPVAc actuation range. The mean absolute error percentage was calculated as 5.24 ± 2.66%.

(Fig. 10). The absolute error percentage observed in the sensor feedback is presented in Fig. 13. The mean absolute error percentage was $5.24 \pm 2.66\%$.

I. LPVAc DISPLACEMENT CONTROL USING THE PROPOSED SENSOR

The experimental setup shown in Fig.14 was used to evaluate the performance of the proposed integrated sensor in actuator displacement control. A microcontroller development board (mega2560, Arduino) was used as the main controller. Two relay-driven solenoid-actuated open/close flow control

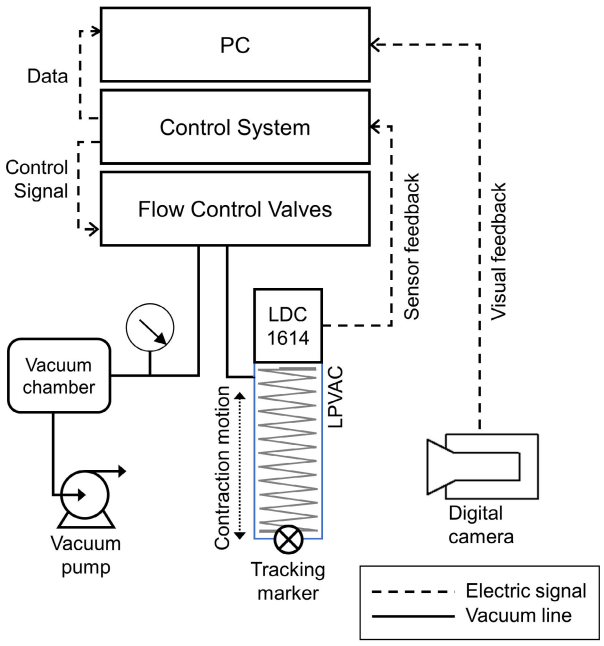

FIGURE 14. The experimental setup used for feedback control performance evaluation.

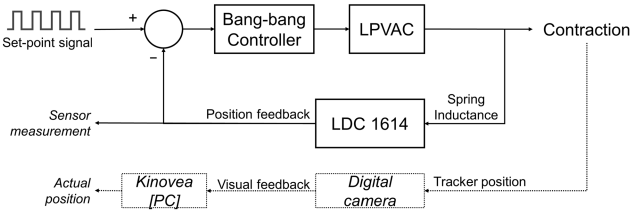

FIGURE 15. The control system used for feedback control performance evaluation.

valves (FCVs) (Dorman, 911-707) were used to separately connect the actuator to the vacuum source for actuation, and the atmosphere for release. The position feedback from the integrated sensor (LDC1614, Texas Instruments) was fed into a bang-bang type controller running on the microcontroller with lower and upper thresholds to control the LPVAc. The feedback control system block diagram is shown in Fig. 15. The sensor feedback data obtained via I2C from the sensing module was serially transferred to and saved on the PC.

A square wave position reference signal was used in the experiment. The square wave had a 20 mm amplitude and 0.25 Hz frequency. The LPVAc was actuated within the calibrated range, between 5 mm and 25 mm. The LPVAc displacement value from the sensor was calculated using the characteristic equation obtained earlier in (5). A marker on the LPVAc was used to measure the actual LPVAc displacement using a digital camera. This visual feedback was post-processed using a digital video analyzing software (Kinovea, ver. 0.8.15) on a PC. The collected data were smoothed using a third-order Savitzky–Golay filter, with a filter length of 21 [55].

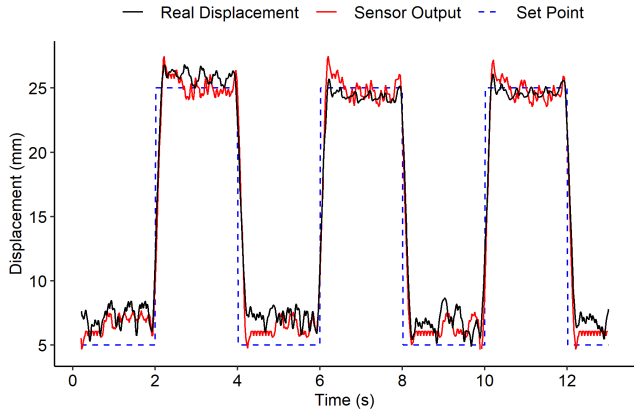

FIGURE 16. The observed sensor response and actual displacement during the feedback control test of the actuator.

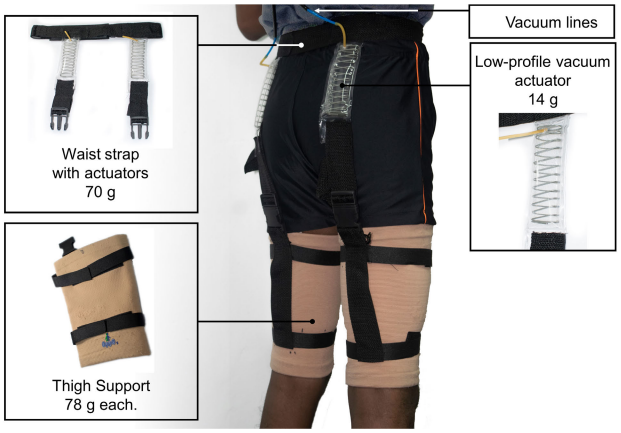

FIGURE 17. The hardware components of the preliminary STSt-assist exosuit and their weight.

The feedback control experiment results are shown in Fig. 16. The input signal is given blue, the sensor feedback signal is given in red, and the actual position of the LPVAc is given in black. The results show that the proposed sensor can be used for effective feedback control of the LPVAc. The sensor is able to closely measure the actual position of the LPVAc and allows the controller to move the LPVAc in the desired square wave motion.

V. USING THE LPVAc IN A PROTOTYPE STSt-ASSIST EXOSUIT

A. EXOSUIT DESIGN

Hip and knee extension are the primary body motions associated with effective STSt. The quadriceps femoris (QF) and the gluteus maximus (GM) are the major muscles recruited during this motion. Between these two muscles groups, the larger GM muscles supply the majority of the anti-gravity lifting force [56]. Hence, we propose the use of an artificial muscle in tandem with the GM to provide assistance during STSt. This requires the assistive actuator, the proposed LPVAc in this case, to be fixed in parallel with the GM muscle of the wearer in a mono-articular design. To evaluate the use of the novel LPVAc in STSt-assist, we designed and developed a novel exosuit prototype. The developed prototype soft exosuit is shown in Fig. 17.

Recent literature presents the Wehner suit [10] as a good basis for soft exosuit design. It describes the use of actual (key) and virtual anchor points to deliver forces across the lower limbs using lines of non-extension. In the proposed design, the LPVAc is fixed in parallel to the GM muscle on the posterior side. A webbing belt worn at the hip acts as one anchor point and a thigh support is used as the other. Here, flexible, and inextensible webbing straps (25 mm wide) are used as anchors and force guides. The proximal anchor point of the LPVAc is the hip worn belt using a sewn-on webbing strap. The LPVAc is distally anchored between the knee and the hip using a soft fabric thigh support sleeve (2040, Oppo Medical, USA). As the thigh support has some amount of slip to allow it to be easily worn, two Velcro-based straps are used

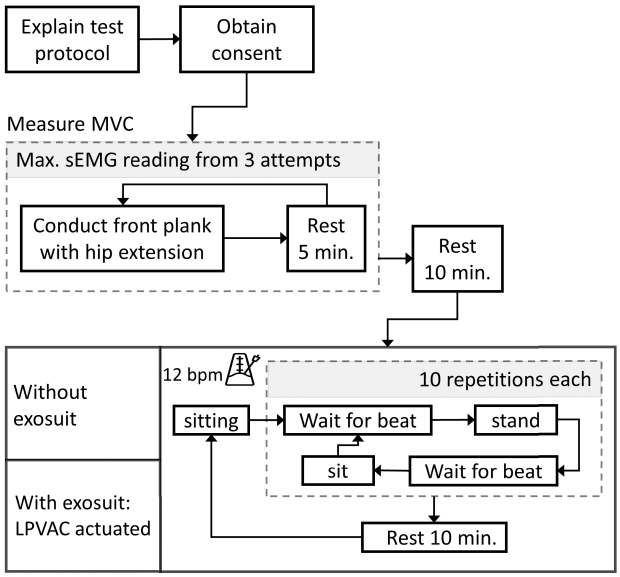

FIGURE 18. An overview of the test protocol used in the exosuit testing.

to tighten the thigh support at the top and the bottom of the sleeve, to limit it slipping along the thigh. Another webbing strap is placed in parallel to the biceps femoris muscles connecting the two tightening straps to guide the applied force. A single LPVAc unit is attached per leg. The distal connections include a quick-release buckle to assist with easy donning and doffing as well as to provide adjustability based on the wearers' height.

The prototype exosuit has a total weight of 324 g, excluding the weight of the vacuum pump, chamber, and valves. The developed exosuit and the weights of each subassembly are shown in Fig. 17. The larger portion of the weight of the suit is worn on the hips, near the body center of mass, hence limiting the metabolic penalty and biomechanical restrictions to motion. Fig. 17 shows the exosuit worn while standing. The LPVAc poses no obstruction to normal seated posture as can be seen from Fig. 20.

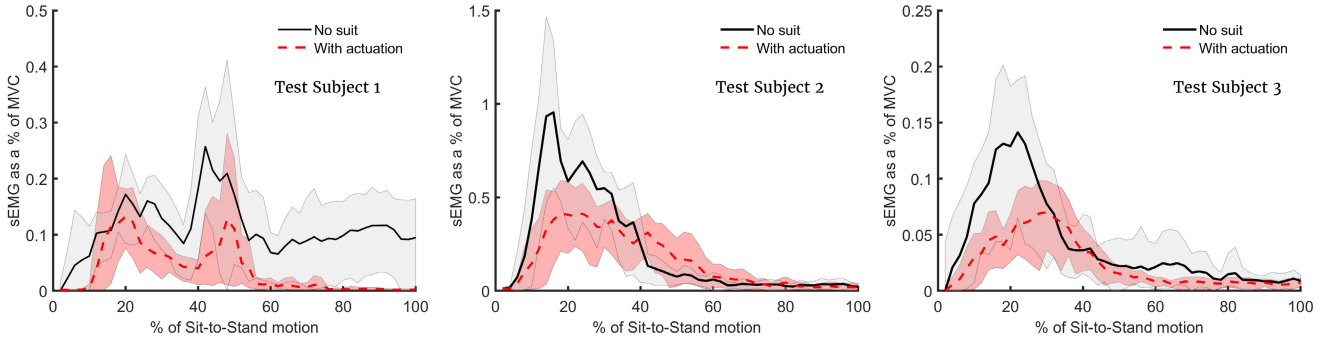

FIGURE 19. The observed reduction in sEMG of GM muscles in three test subjects. The shaded area depicts the range of maximum and minimum readings obtained at each position of the STSt motion over 10 repetitions.

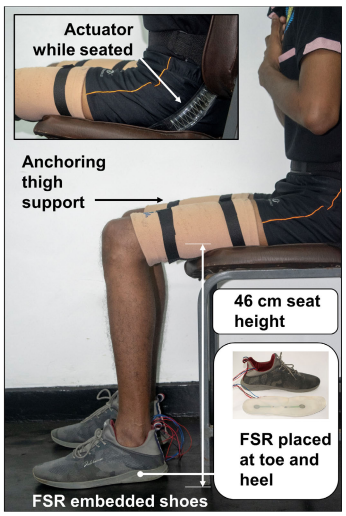

FIGURE 20. The experimental setup for STSt. FSR embedded shoes are worn to measure toe and heal ground forces. Inset shows the non-obtrusiveness of the proposed actuator while seated.

B. EXOSUIT TESTING

Healthy volunteers were recruited to test the effectiveness of the proposed exosuit in assisting STSt. Three healthy volunteers (see Table 3 for details) took part in the trials. The test protocol is shown in Fig. 18. Initially, the test procedure was explained in detail, and informed written consent was obtained from each volunteer. Each subject went through a guided trial run before each experiment. Secondly, Each volunteer was asked to do a front plank with hip extension as given in [57] to obtain the maximum voluntary contraction (MVC) value of GM. Three trials were conducted for each volunteer, and the maximum value was recorded as that subject's GM MVC. Thirdly, the trials were conducted in two parts; without the exosuit and with the exosuit and the LPVAc actuated. In each part, the volunteer carried out 10 iterations of STSt. The test subjects wore clothing similar to the suited condition, during the no-suit test as well. The subjects were instructed to follow a 12-bpm metronome in carrying out the transitions.

The chair height for the experiment was set to 46 cm, following the DIN 18040-1 design guidelines for public restrooms. The STSt was identified by measuring ground reaction force using force sensing resistors integrated to the test subjects insole, at the toe and the heel per foot at 100 Hz (see Fig. 20). Surface electromyography (sEMG) was used to measure the GM muscle activity during STSt. As this exosuit test was carried out to evaluate the applicability of the LPVAc in driving an STSt-assist exosuit, the LPVAcs were driven in open-loop without the use of sensor feedback.

TABLE 3. Test subject details and observed sEMG signal reduction.

Subject (m/f)	Age (Y)	Weight (kg)	Height (m)	BMI (kg/m^2)	Reduction (%)
1 (m)	26	45	1.65	16.5	66.93
2 (m)	27	64	1.65	23.5	42.28
3 (m)	27	65	1.60	25.4	26.72
mean ± SD [%]					45.31 ± 20.28

C. EMG DATA ANALYSIS

Surface EMG data were collected from the GM muscles of both legs, and the data from the dominant leg was selected for the analysis. A Bagnoli desktop EMG system (Delsys, Inc., USA) was used for the sEMG data acquisition. The acquired data was initially captured, recorded, and processed using the EMGworks software (Delsys, Inc., USA). The Bagnoli system acquired the sEMG data at 4 kHz, and this raw data stream was smoothed to obtain the RMS value with a 250-sample window. This provided a 16 Hz output signal which was post-processed in MATLAB. The mean of ten sit-to-stand repetitions, for powered suit and without suit tests, were averaged and normalized for each muscle with respect to its MVC value.

The mean values of the RMS'd sEMG obtained for each of the two conditions (without suit and suit worn and LPVAc actuated) were then DC offset, by subtracting the minimum of each condition from itself. The STSt time was normalized to a 100 % cycle between the maximum gradients observed in the toe and heel ground reaction force sensors. These normalizations were carried out as post-processing. The results of this analysis for the three healthy volunteer subjects are shown in Fig. 19.

To evaluate the effectiveness of the provided assistance via the exosuit, the percentage reduction in the area under the GM muscle activity curves in Fig. 19 was calculated. The obtained results indicate a mean muscle activity reduction of 45 % during STSt. This is comparable to results shown in [17]. The variance of the muscle activity reduction can be attributed to the different builds of the volunteers (see Table 3). Hence, we can conclude that the prototype soft exosuit driven by the proposed LPVAc can effectively assist in reducing the muscle activity requirement during STSt.

VI. CONCLUSION

Patients wheel/chair bound following muscle weakness need to be encouraged to break their sedentary behavior and attempt independent motion. A soft exosuit, driven by non-obstructive low-profile actuators, that can be worn while seated can be used in such instances to encourage such patients to frequently and easily transition from sit-to-stand. To facilitate this, a novel low-profile actuator with an integrated displacement sensor is developed, tested, and integrated into a wearable soft exosuit. The proposed actuator comprises of low-profile spring encased within a polyethylene film pouch that contracts longitudinally when the air within the pouch is evacuated. Characterization of the actuator is carried out to determine the capability of actuation. Experimental results show that this lightweight (14 g) actuator is capable of lifting 285 times its self-weight, and deliver 65% maximum strain at no load. Rapid contraction is an advantage in this actuator due to vacuum actuation, and it incorporates a faster self-return to the initial state aided by the spring.

A key limitation in contemporary soft actuators is the absence of accurate sensory feedback. This is overcome in the proposed design by the integration of an inductive displacement sensing method, which shows promising results. This proposed sensor is able to perform effectively with minimal disturbance to the actuator motion. The proposed inductance sensing module displayed high linearity with the displacement of the LPVAc. The experimental analysis further presented a sensitivity of 0.0022 $\mu H/mm$, a hysteresis of 1.49 %, and an average absolute error percentage of 5.24 $\pm$ 2.66 %. The sensor showed good repeatability, with a minimum standard deviation of 1.65 mm, in the repeated measurement of a setpoint. The repeatability was seen to be higher at larger displacements. The proposed sensor showed effectiveness in being used as a feedback sensor in position control of the LPVAc. Key characteristics of the developed PAM and the integrated sensor are listed in Table. 4.

The proposed actuator is used to drive a novel hip and knee flexion-assist mono-articular exosuit. This preliminary exosuit design is used to validate the applicability of the developed actuator. sEMG data collected from the GM muscles during STSt show successful mean muscle activity reduction >45% for suit with actuation condition versus the no suit condition. Therefore, this work shows potential for further development. As the developed actuator and the exosuit is in their preliminary stages, the authors plan to carry out further development and testing using multiple persons with diagnosed muscle weaknesses.

TABLE 4. The characteristics of the proposed LPVAc and its integrated sensor.

	Measure	Value
Actuator	Min. cross-section	10 mm x 40 mm
	Min. Weight	14 g
	Max. force	39.05 N
	Max. stress	103.2 kPa
	Max. strain	65 %
	Force-to-weight ratio	285
Sensor	Sensitivity	0.0022 $\mu H/mm$
	Resolution	10 nH
	Hysteresis	1.49 %
	Average Error (abs.)	5.24 $\pm$ 2.66 %

Few limitations are present in this proposed design. The maximum applicable blocked force is limited by the maximum applicable differential pressure, which is limited to a single atmosphere under normal conditions. The presence of strong magnetic fields in the vicinity of the actuator can affect the performance of the displacement sensor. However, as part of a wearable system this limitation does not appear to be a critical issue. As future work, the authors plan, to increase the number of test subjects used for the exosuit performance evaluation including actual patients, to miniaturize the proposed actuator for easier integration to more complex wearable systems, and to improve the feedback control system for improved displacement control.

ACKNOWLEDGMENT

The publication support was provided from the conference and publication support scheme of Senate Research Committee, University of Moratuwa.

REFERENCES

[1] W. Brie, "Consideration of function & functional decline," in *Current Diagnosis and Treatment: Geriatrics*, B. A. Williams, A. Chang, C. Ahalt, H. Chen, R. Conant, C. S. Landefeld, C. Ritchie, and M. Yukawa, Eds., 2nd ed. New York, NY, USA: McGraw-Hill, 2014, pp. 3–4.

[2] E. T. Yümin, T. T. Şimşek, M. Sertel, A. Öztürk, and M. Yümin, "The effect of functional mobility and balance on health-related quality of life (HRQoL) among elderly people living at home and those living in nursing home," *Arch. Gerontol. Geriatrics*, vol. 52, no. 3, pp. e180–e184, May 2011.

[3] V. Bartenbach, K. Schmidt, M. Naef, D. Wyss, and R. Riener, "Concept of a soft exosuit for the support of leg function in rehabilitation," in *Proc. IEEE Int. Conf. Rehabil. Robot. (ICORR)*, Aug. 2015, pp. 125–130.

[4] H. Herr, "Exoskeletons and orthoses: Classification, design challenges and future directions," *J. Neuroeng. Rehabil.*, vol. 6, p. 21, Dec. 2009.

[5] B. Chen, H. Ma, L.-Y. Qin, F. Gao, K.-M. Chan, S.-W. Law, L. Qin, and W.-H. Liao, "Recent developments and challenges of lower extremity exoskeletons," *J. Orthopaedic Transl.*, vol. 5, pp. 26–37, Apr. 2016.

[6] R. K. P. S. Ranaweera, W. A. T. I. Jayasiri, W. G. D. Tharaka, J. H. H. P. Gunasiri, R. A. R. C. Gopura, T. S. S. Jayawardena, and G. K. I. Mann, "Anthro-X: Anthropomorphic lower extremity exoskeleton robot for power assistance," in *Proc. 4th Int. Conf. Control, Automat. Robot. (ICCAR)*, Apr. 2018, pp. 82–87.

[7] S. Rossi, A. Colazza, M. Petrarca, E. Castelli, P. Cappa, and H. I. Krebs, "Feasibility study of a wearable exoskeleton for children: Is the gait altered by adding masses on lower limbs?" *PLoS ONE*, vol. 8, no. 9, Sep. 2013, Art. no. e73139.

[8] A. Schiele, "Ergonomics of exoskeletons: Objective performance metrics," in *Proc. World Haptics 3rd Joint EuroHaptics Conf. Symp. Haptic Interfaces Virtual Environ. Teleoperator Syst.*, Mar. 2009, pp. 103–108.
[9] M. Cianchetti, C. Laschi, A. Menciassi, and P. Dario, "Biomedical applications of soft robotics," *Nature Rev. Mater.*, vol. 3, pp. 143–153, Jun. 2018.
[10] M. Wehner, B. Quinlivan, P. M. Aubin, E. Martinez-Villalpando, M. Baumann, L. Stirling, K. Holt, R. Wood, and C. Walsh, "A lightweight soft exosuit for gait assistance," in *Proc. IEEE Int. Conf. Robot. Automat.*, May 2013, pp. 3362–3369.
[11] A. T. Asbeck, S. M. M. D. Rossi, K. G. Holt, and C. J. Walsh, "A biologically inspired soft exosuit for walking assistance," *Int. J. Robot. Res.*, vol. 34, no. 6, pp. 744–762, May 2015.
[12] J. Bae, C. Siviy, M. Rouleau, N. Menard, K. Odonnell, I. Geliana, M. Athanassiu, D. Ryan, C. Bibeau, L. Sloot, P. Kudzia, T. Ellis, L. Awad, and C. J. Walsh, "A lightweight and efficient portable soft exosuit for paretic ankle assistance in walking after stroke," in *Proc. IEEE Int. Conf. Robot. Automat. (ICRA)*, May 2018, pp. 2820–2827.
[13] Y.-L. Park, B.-R. Chen, N. O. Pérez-Arancibia, D. Young, L. Stirling, R. J. Wood, E. C. Goldfield, and R. Nagpal, "Design and control of a bio-inspired soft wearable robotic device for ankle–foot rehabilitation," *Bioinspiration Biomimetics*, vol. 9, no. 1, Jan. 2014, Art. no. 016007.
[14] T. Kawamura, K. Takanaka, T. Nakamura, and H. Osumi, "Development of an orthosis for walking assistance using pneumatic artificial muscle: A quantitative assessment of the effect of assistance," in *Proc. IEEE 13th Int. Conf. Rehabil. Robot. (ICORR)*, Jun. 2013, pp. 1–6.
[15] S. Jin, S. Guo, H. Kazunobu, X. Xiong, and M. Yamamoto, "Influence of a soft robotic suit on metabolic cost in long-distance level and inclined walking," *Appl. Bionics Biomech.*, vol. 2018, pp. 1–8, Jul. 2018.
[16] Y. Li and M. Hashimoto, "Design and prototyping of a novel lightweight walking assist wear using PVC gel soft actuators," *Sens. Actuators A, Phys.*, vol. 239, pp. 26–44, Mar. 2016.
[17] K. Schmidt, J. E. Duarte, M. Grimmer, A. Sancho-Puchades, H. Wei, C. S. Easthope, and R. Riener, "The myosuit: Bi-articular anti-gravity exosuit that reduces hip extensor activity in sitting transfers," *Frontiers Neurorobot.*, vol. 11, pp. 1–16, Oct. 2017.
[18] A. L. Kulasekera, R. B. Arumathanthri, D. S. Chathuranga, T. D. Lalitharatne, and R. C. Gopura, "A low-profile vacuum actuator: Towards a sit-to-stand assist exosuit," in *Proc. 3rd IEEE Int. Conf. Soft Robot. (RoboSoft)*, May 2020, pp. 110–115.
[19] R. B. Arumathanthri, A. L. Kulasekera, and D. S. Chathuranga, "An induction type displacement sensor used in a novel soft robotic muscle actuator," in *Proc. Int. Conf. Image Process. Robot. (ICIP)*, Mar. 2020, pp. 1–6.
[20] C. Majidi, "Soft robotics: A perspective—Current trends and prospects for the future," *Soft Robot.*, vol. 1, no. 1, pp. 5–11, Mar. 2014.
[21] D. Rus and M. T. Tolley, "Design, fabrication and control of soft robots," *Nature*, vol. 521, pp. 467–475, May 2015.
[22] Z. Wang, D. S. Chathuranga, and S. Hirai, "3D printed soft gripper for automatic lunch box packing," in *Proc. IEEE Int. Conf. Robot. Biomimetics (ROBIO)*, Dec. 2016, pp. 503–508.
[23] C. Lee, M. Kim, Y. J. Kim, N. Hong, S. Ryu, H. J. Kim, and S. Kim, "Soft robot review," *Int. J. Control, Autom. Syst.*, vol. 15, no. 1, pp. 3–15, Feb. 2017.
[24] C.-P. Chou and B. Hannaford, "Measurement and modeling of McKibben pneumatic artificial muscles," *IEEE Trans. Robot. Autom.*, vol. 12, no. 1, pp. 90–102, Feb. 1996.
[25] M. F. Cullinan, E. Bourke, K. Kelly, and C. McGinn, "A Mckibben type sleeve pneumatic muscle and integrated mechanism for improved stroke length," *J. Mech. Robot.*, vol. 9, no. 1, Feb. 2017.
[26] T. Nakamura and H. Shinohara, "Position and force control based on mathematical models of pneumatic artificial muscles reinforced by straight glass fibers," in *Proc. IEEE Int. Conf. Robot. Automat.*, Apr. 2007, pp. 4361–4366.
[27] Y. Sun, J. Guo, T. M. Miller-Jackson, X. Liang, M. H. Ang, and R. C. H. Yeow, "Design and fabrication of a shape-morphing soft pneumatic actuator: Soft robotic pad," in *Proc. IEEE/RSJ Int. Conf. Intell. Robots Syst. (IROS)*, Sep. 2017, pp. 6214–6220.
[28] D. Sasaki, T. Noritsugu, and M. Takaiwa, "Development of active support splint driven by pneumatic soft actuator (ASSIST)," in *Proc. IEEE Int. Conf. Robot. Automat.*, Apr. 2005, pp. 520–525.
[29] J. Wirekoh and Y.-L. Park, "Design of flat pneumatic artificial muscles," *Smart Mater. Struct.*, vol. 26, no. 3, Mar. 2017, Art. no. 035009.
[30] S. Kurumaya, H. Nabae, G. Endo, and K. Suzumori, "Design of thin McKibben muscle and multifilament structure," *Sens. Actuator A, Phys.*, vol. 261, pp. 66–74, Jul. 2017.
[31] F. Daerden and D. Lefeber, "The concept and design of pleated pneumatic artificial muscles," *Int. J. Fluid Power*, vol. 2, no. 3, pp. 41–50, Jan. 2001.
[32] Y.-L. Park, J. Santos, K. G. Galloway, E. C. Goldfield, and R. J. Wood, "A soft wearable robotic device for active knee motions using flat pneumatic artificial muscles," in *Proc. IEEE Int. Conf. Robot. Automat. (ICRA)*, May 2014, pp. 4805–4810.
[33] T. Noritsugu, M. Takaiwa, and D. Sasaki, "Power assist wear driven with pneumatic rubber artificial muscles," in *Proc. 15th Int. Conf. Mechatronics Mach. Vis. Pract.*, Dec. 2008, pp. 539–544.
[34] A.-F. Hassanin, D. Steve, and N.-M. Samia, "A novel, soft, bending actuator for use in power assist and rehabilitation exoskeletons," in *Proc. IEEE/RSJ Int. Conf. Intell. Robots Syst. (IROS)*, Sep. 2017, pp. 533–538.
[35] D. P. Ferris, J. M. Czerniecki, and B. Hannaford, "An ankle-foot orthosis powered by artificial pneumatic muscles," *J. Appl. Biomech.*, vol. 21, no. 2, pp. 189–197, May 2005.
[36] A. J. Young and D. P. Ferris, "State of the art and future directions for lower limb robotic exoskeletons," *IEEE Trans. Neural Syst. Rehabil. Eng.*, vol. 25, no. 2, pp. 171–182, Feb. 2017.
[37] F. Daerden and D. Lefeber, "Pneumatic artificial muscles: Actuators for robotics and automation," *Eur. J. Mech. Environ. Eng.*, vol. 47, no. 1, pp. 10–21, 2000.
[38] H. P. H. Anh, C. Van Kien, and N. T. Nam, "Advanced force control of the 2-axes PAM-based manipulator using adaptive neural networks," *Robotica*, vol. 36, no. 9, pp. 1333–1362, Sep. 2018.
[39] D. Yang, M. S. Verma, J.-H. So, B. Mosadegh, C. Keplinger, B. Lee, F. Khashai, E. Lossner, Z. Suo, and G. M. Whitesides, "Buckling pneumatic linear actuators inspired by muscle," *Adv. Mater. Technol.*, vol. 1, no. 3, Jun. 2016, Art. no. 1600055.
[40] S. Li, D. M. Vogt, D. Rus, and R. J. Wood, "Fluid-driven origami-inspired artificial muscles," *Proc. Nat. Acad. Sci. USA*, vol. 114, no. 50, pp. 13132–13137, Dec. 2017.
[41] N. S. Usevitch, A. M. Okamura, and E. W. Hawkes, "APAM: Antagonistic pneumatic artificial muscle," in *Proc. IEEE Int. Conf. Robot. Automat. (ICRA)*, Brisbane, QLD, Australia, May 2018, pp. 1539–1546.
[42] S. D. Katugampala, K. M. S. Arachchi, S. Asanka, R. B. Arumathanthri, A. L. Kulasekera, and N. D. Jayaweera, "Design and characterization of a novel vacuum bending actuator and a bimorph: For preliminary use in a continuum robot arm," in *Proc. IEEE Int. Conf. Cybern. Intell. Syst. (CIS) IEEE Conf. Robot., Automat. Mechatronics (RAM)*, Bangkok, Thailand, Nov. 2019, pp. 263–268.
[43] G. Agarwal, M. A. Robertson, H. Sonar, and J. Paik, "Design and computational modeling of a modular, compliant robotic assembly for human lumbar unit and spinal cord assistance," *Sci. Rep.*, vol. 7, no. 1, pp. 1–11, Dec. 2017.
[44] J.-G. Lee and H. Rodrigue, "Origami-based vacuum pneumatic artificial muscles with large contraction ratios," *Soft Robot.*, vol. 6, no. 1, pp. 109–117, Feb. 2019.
[45] H. Herr and R. Kornbluh, "New horizons for orthotic and prosthetic technology: Artificial muscle for ambulation," in *Proc. Smart Struct. Mater., Electroactive Polym. Actuat. Devices (EAPAD)*, 2004, doi: 10.1117/12.544510.
[46] R. B. Arumathanthri, B. S. K. Abeygoonawardana, I. D. C. D. Kumarasinghe, D. S. Chathuranga, T. D. Lalitharatne, and A. L. Kulasekera, "A soft robotic gripper with sensory feedback fabricated by latex using coagulant dipping process," in *Proc. IEEE Int. Conf. Robot. Biomimetics (ROBIO)*, Dec. 2018, pp. 2082–2087.
[47] D. G. Caldwell, G. A. Medrano-Cerda, and M. J. Goodwin, "Braided pneumatic actuator control of a multi-jointed manipulator," in *Proc. IEEE Syst. Man Cybern. Conf. (SMC)*, Oct. 1993, pp. 423–428.
[48] M. C. Yuen, R. Kramer-Bottiglio, and J. Paik, "Strain sensor-embedded soft pneumatic actuators for extension and bending feedback," in *Proc. IEEE Int. Conf. Soft Robot. (RoboSoft)*, Apr. 2018, pp. 202–207.
[49] A. Hildebrandt, O. Sawodny, R. Neumann, and A. Hartmann, "Cascaded control concept of a robot with two degrees of freedom driven by four artificial pneumatic muscle actuators," in *Proc. Amer. Control Conf.*, Jun. 2005, pp. 680–685.
[50] N. Farrow and N. Correll, "A soft pneumatic actuator that can sense grasp and touch," in *Proc. IEEE/RSJ Int. Conf. Intell. Robots Syst. (IROS)*, Sep. 2015, pp. 2317–2323.
[51] J. Morrow, H.-S. Shin, C. Phillips-Grafflin, S.-H. Jang, J. Torrey, R. Larkins, S. Dang, Y.-L. Park, and D. Berenson, "Improving soft pneumatic actuator fingers through integration of soft sensors, position and force control, and rigid fingernails," in *Proc. IEEE Int. Conf. Robot. Automat. (ICRA)*, May 2016, pp. 5024–5031.

[52] W. Felt, S. Lu, and C. D. Remy, "Modeling and design of 'smart braid' inductance sensors for fiber-reinforced elastomeric enclosures," *IEEE Sensors J.*, vol. 18, no. 7, pp. 2827–2835, Apr. 2018.
[53] *LDC1612, LDC1614 Multi-Channel 28-Bit Inductance to Digital Converter (LDC) for Inductive Sensing*, LDC1614 Datasheet, Dallas, TX, USA, Texas Instruments, Dec. 2014.
[54] A. N. Chaudhury and D. Datta, "Analysis of prismatic springs of non-circular coil shape and non-prismatic springs of circular coil shape by analytical and finite element methods," *J. Comput. Design Eng.*, vol. 4, no. 3, pp. 178–191, Jul. 2017.
[55] S. R. Krishnan and C. S. Seelamantula, "On the selection of optimum Savitzky-Golay filters," *IEEE Trans. Signal Process.*, vol. 61, no. 2, pp. 380–391, Jan. 2013.
[56] M. E. Roebroeck, C. A. M. Doorenbosch, J. Harlaar, R. Jacobs, and G. J. Lankhorst, "Biomechanics and muscular activity during sit-to-stand transfer," *Clin. Biomech.*, vol. 9, no. 4, pp. 235–244, Jul. 1994.
[57] K. Boren, C. Conrey, J. L. Coguic, L. Paprocki, M. Voight, and T. K. Robinson, "Electromyographic analysis of gluteus medius and gluteus maximus during rehabilitation exercises," *Int. J. Sports Phys. therapy*, vol. 6, no. 3, pp. 23–206, 2011.

ASITHA L. KULASEKERA (Member, IEEE) received the B.Sc. (Hons.) and M.Sc. degrees in mechanical engineering from the University of Moratuwa (UoM), Sri Lanka, in 2010 and 2012, respectively, where he is currently pursuing the Ph.D. degree in mechanical engineering with the Computational Sensing and Smart Machines Laboratory, Department of Mechanical Engineering. Since 2012, he has been a Lecturer with the Department of Mechanical Engineering, UoM. He has published more than 45 peer-reviewed journal and conference papers. His research interests include soft robotics, bio-robotics, mechatronics, and systems engineering.

RANCIMAL B. ARUMATHANTHRI received the B.Sc. (Hons.) and M.Sc. degrees in mechanical engineering from the University of Moratuwa (UoM), Sri Lanka, in 2018 and 2021, respectively. From 2018 to 2019, he was a Research Assistant with the Computational Sensing and Smart Machines Laboratory, Department of Mechanical Engineering, UoM. He is currently working as a Lecturer with the Institute of Technology, UoM. His research interests include soft robotics, development of soft actuators, soft sensors, and soft exoskeletons. In 2018, he was awarded the overseas conference travel grant under the Thomas Andrew Common Grants Scheme from the Institute of Mechanical Engineers, U.K.

DAMITH S. CHATHURANGA (Member, IEEE) received the B.Sc. degree (Hons.) in mechanical engineering from the University of Moratuwa (UoM), Sri Lanka, in 2009, and the M.E. and Ph.D. degrees in robotics engineering from Ritsumeikan University, Japan, in 2013 and 2016, respectively. Since 2016, he has been a Senior Lecturer with the Department of Mechanical Engineering, UoM. Since 2021, he has also been the Director of the Center for Advanced Robotics, UoM. He has published more than 30 peer-reviewed articles. His research interests include soft robotics, tactile sensors, and bio-robotics.

R. A. R. C. GOPURA (Senior Member, IEEE) received the B.Sc. degree (Hons.) in engineering and the M.Eng. degree from the University of Moratuwa (UoM), Sri Lanka, and the Ph.D. degree in robotics and intelligent systems from Saga University, Japan, in 2009. He carried out his Postdoctoral Research with Saga University. He was the Head of the Department of Mechanical Engineering, UoM, from 2017 to 2020. He is currently working as a Professor with the Department of Mechanical Engineering, the Head of the Department of Medical Technology, the Director, and a Research with UoM. He has published more than 110 peer-reviewed journal and conference papers. His research interests include bio-mechatronics, exoskeleton robots, and robotic prostheses. He was the Chairman of the IEEE Robotics and Automation Society Sri Lanka Section Chapter, from 2017 to 2020, and the IEEE Sri Lanka Section, in 2020.

THILINA D. LALITHARATNE (Member, IEEE) received the B.Sc. degree (Hons.) in mechanical engineering and the M.Sc. degree in electronics and automation from the University of Moratuwa (UoM), Sri Lanka, in 2009 and 2013, respectively, and the Ph.D. degree in robotics and intelligent systems from Saga University, Japan, in 2014. From 2015 to 2019, he was a Senior Lecturer with the Department of Mechanical Engineering, UoM. He is currently a Postdoctoral Research Associate with the Morph Laboratory, Dyson School of Design Engineering, Imperial College London, and a Visiting Researcher with the Bio-Inspired Robotics Laboratory (BIRL), University of Cambridge. He has published more than 50 peer-reviewed articles. His research interests include human–machine-interaction, soft robotics, brain–computer interface, bio-robotics, and mechatronics. His awards and honors include the BCI Award and the First place winner awards in International Brain Machine Interface (BMI) Hackathons from SMC2017 and BIBE2019.